July 2018

Thermal Performance Evaluation of a Residential Solar/Gas Hybrid Water Heating System

Saroj Karki
Oregon State University, United States of America, karkis@oregonstate.edu

Karl R. Haapala
Oregon State University, United States of America, karl.haapala@oregonstate.edu

Brian M. Fronk
Oregon State University, United States of America, brian.fronk@oregonstate.edu

Thermal Performance Evaluation of a Solar/Gas
Hybrid Water Heating System

Saroj KARKI[1], Karl R. HAAPALA[1], Brian M. FRONK[1]*

School of Mechanical, Industrial and Manufacturing Engineering
Oregon State University
Corvallis, OR, United States
541-737-3952, brian.fronk@oregonstate.edu

* Corresponding Author

ABSTRACT

In climate regions with large seasonal variations in solar radiation, such as the Pacific Northwest, a solar energy collector might not economically satisfy year-round domestic water heating demands, requiring an auxiliary unit, such as a natural gas-fired water heater. Previous studies have shown that the burner efficiency of a gas-fired water heater varies depending on the log-mean temperature difference between cold fluid (water) and hot fluid (combustion gases). In a solar/gas hybrid water heating system where a solar collector is used in conjunction with a gas-fired heater, the partial heating of water provided by the solar input reduces the log-mean temperature difference value for gas heater, reducing the efficiency of gas burner. Since this efficiency reduction varies depending on the amount of pre-heating provided by solar input, it is difficult to accurately predict the actual cost and energy savings offered by a solar/gas hybrid water heater. Hence, to predict the actual energy and cost savings under various design conditions, the performance of solar/gas hybrid systems must be better understood. The purpose of this work is to experimentally determine the thermal performance of a solar/gas water hybrid water heating system with a 6.44 m^2 flat plate solar collector array and a 22.3 kW natural gas burner. Under different temperature lifts and solar insolation values, the system was operated at three different modes of heating: solar, gas, and combined solar/gas mode. Efficiency value for each mode is calculated. Based on the experimental efficiency results, a configuration that would provide higher efficiency for combined solar/gas heating is suggested.

1. INTRODUCTION

Solar water heating systems (SWHS) are a simple and cost-effective renewable technology for harnessing the sun's energy to generate hot water. A SWHS typically consists of a solar collector, a hot water storage tank, and a control system. The operating principle is that the solar collector absorbs the incident solar radiation and transfers the energy to a working fluid flowing inside the collector tubes. The energy carried by the working fluid can be used either directly in the form of hot water, or to charge a thermal energy storage tank from where energy can be drawn for use later. A flat-plate collector (FPC) is the most common type of solar collector used for harvesting solar energy at relatively low fluid temperatures, and has seen commercial application around the world (Duffie & Beckman, 2013). It consists of a selective flat plate absorber covered by a transparent glass or plastic cover (glazing), tubes to circulate the heat transfer fluid within the body of the collector, and insulation to minimize heat loss from the sides and bottom of the absorber plate (Kalogirou, 2013). The percentage of water heating energy required by a household that is provided by the solar collectors is quantified in terms of solar fraction (Kalogirou, 2013). Due to the diurnal and seasonal variation of available solar energy, an auxiliary heating source is generally necessary to provide backup heating whenever solar energy fails to meet the hot water demand (Duffie & Beckman, 2013). Electric resistance heaters are the most commonly used backup energy source.

Numerous experimental studies have been carried out over the years to analyze the thermal performance of FPCs under real weather conditions. Rodriguez-Hidalgo *et al.* (2012) carried out an experimental study of a 50 m^2 FPC in Madrid, Spain to quantify the sensitivity of instantaneous thermal performance of solar collectors to the following factors: wind thermal loss, collector aging, thermal capacitance, irradiance incidence angle, and radiation losses. Michaelides & Eleftheriou (2011) studied the thermal performance of a solar water heating system with a 3 m^2 FPC and 68 L storage tank under real weather conditions in Cyprus for 2 years and found that the annual average daily performance of the system was relatively insensitive to solar radiation fluctuations ranging from 800 to 1100 W m^{-2}. Ayompe & Duffy (2013) experimentally measured the thermal performance of a solar water heating system with 4 m^2

FPCs located in Dublin, Ireland and reported annual average daily solar fraction of 32.2%, collector efficiency of 45.6%, and overall system efficiency of 37.8%. In all above-mentioned studies, an electric immersion heater is used as the auxiliary energy source. Electric resistance heaters are nearly 100% efficient, meaning all the input electric energy is converted into heat and supplied to the water. This conversion efficiency is not dependent on the temperature of the heated water. Since the efficiency of electric heating is constant, it is straight-forward to predict the cost and energy of the required auxiliary energy if the solar fraction is known. However, with natural gas-fired water heating systems, the efficiency varies depending on the amount of heat transferred in the heat exchanger, which is directly impacted by the temperature difference between cold fluid (water) and hot fluid (combustion gases).

Presently, the cost of natural gas in US is below the cost of electricity on a kWh-to-kWh basis (EIA, 2018), making natural gas backup an attractive option in terms of auxiliary energy cost. Furthermore, depending on the feedstock for generating electricity, there may be advantages from carbon emissions and primary energy consumption perspectives in obtaining auxiliary heating directly with gas (Fronk & Keinath, 2017). However, previous studies (ASHRAE, 2008; Maguire, 2012; Makaire & Ngendakumana, 2010) have shown that the efficiency of gas-fired water heaters decreases with increase in inlet water temperature. This is because with increase in inlet water temperature, the temperature driving force between the combustion gases and tank water decreases, reducing the heat transfer rate. In a solar/gas hybrid water heating system where a solar collector is used in conjunction with a gas-fired heater, the partial heating of process fluid provided by the solar input reduces the log-mean temperature difference (LMTD) value for the gas heater, reducing the efficiency of the gas burner. Therefore, lower overall system efficiency than expected may be observed while running a solar/gas hybrid water heating system in a combined solar/gas mode. Since this efficiency varies depending on the amount of pre-heating provided by solar input, it is more challenging to accurately predict the actual cost and energy savings offered by a solar/gas water heater.

Hence, to predict the actual energy and cost savings under various design conditions, the performance of solar/gas hybrid systems must be better understood. The objective of this work is to experimentally determine the thermal performance of a commercial solar/gas water hybrid water heating system with a 6.44 m^2 flat plate solar collector array and a 22.3 kW natural gas burner under representative operating conditions. The system was operated at three different modes of heating: solar only, gas only, and combined solar/gas mode for different temperature lifts and solar insolation values. Efficiency values for each mode were calculated. Based on the experimental efficiency results, a potential configuration that would provide optimal efficiency for the combined solar/gas mode of heating is suggested.

2. EXPERIMENTAL SETUP AND DATA REDUCTION METHODS

2.1 Experimental Setup

An active closed loop hybrid solar thermal water heating system (STWHS) installed on a campus building at Oregon State University in Corvallis, Oregon (44.56° N, 123.27° W), provides the basis for this experimental study. The STWHS consists of a 6.44 m^2 FPC array, a 265 L hot water storage tank, a solar pump, and a commercial control unit. The collector array consists of three Schüco Slim V plus FPCs, each with gross area of 2.32 m^2, connected in series. The collectors are facing south and are inclined at 45 degrees. Each collector has zero loss efficiency rating of 76.7%. The collector heat loss coefficient values, k_1 and k_2, are defined to be 3.71 and 0.016 $Wm^{-2} K^{-1}$, respectively. The absorber plate is made up of copper tubes covered with high selectivity coating that has short-wave absorptivity of 95% and long wave emissivity of 5%. Each collector is covered by a 4-mm thick low iron glazing of 91% transmittance. The side and bottom of the collectors are insulated with a 20-mm mineral wool insulation. The maximum operating temperature and pressure of the collectors are 120°C and 10 bars, respectively. The storage tank is a Schüco S WW 70-1GPN model, made up of stainless steel. It is equipped with an auxiliary 22.27 kW natural gas burner, which has manufacture specified burner efficiency rating of 80% defined using lower heating value. The tank contains an immersed solar heating coil that allow heat transfer between the solar fluid and potable water. The solar coil has heat transfer surface area of 1.31 m^2.

A schematic of the experimental setup is reported in Figure 1. A solution of propylene glycol (40% propylene glycol by mass) is used as the heat transfer fluid to provide freeze protection during colder months. The glycol water mixture is pumped through the FPC array, where it absorbs the incoming solar radiation. The hot glycol water mixture then passes through the solar heating coils inside the storage tank where it exchanges heat with the tank water. The natural gas burner is turned on to top up the tank temperature whenever the solar energy is insufficient to heat the tank to the required temperature of 60±0.5°C. The hot water draw-off system consists of four solenoid valves connected in parallel, each with a different flow restrictor. The array of valves can be actuated in different combinations to achieve 15 distinct flowrates ranging from 0.94 to 16 liters per minute. This arrangement provides the capability to simulate

actual residential hot water draws. The operation and closing operation of the valves is controlled by a program written in LabVIEW software.
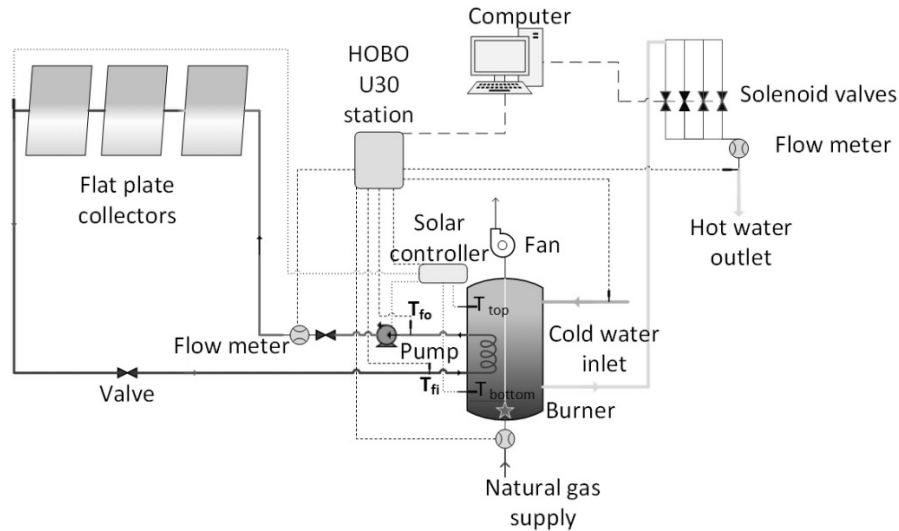
Figure 1: Schematic diagram of the experimental setup

2.2 Instrumentation

The STWHS is equipped with a HOBO U30 station for monitoring and data logging sensors at a specific time interval. The HOBO station is configured with 14 data channels via a plug-in modular connector. The following system parameters are data logged: global solar radiation, collector outlet temperature, temperature of glycol water mixture at the inlet and outlet of the solar coil, water temperature at the top and bottom of the storage tank, cold water (city) inlet temperature, delivered hot water exit temperature, volumetric flow rate of glycol water mixture, and volumetric flow rate of natural gas.

A summary of all instruments data logged is provided in Table 1. All sensors were sampled at a 10-second interval. Physical properties of the fluid, such as density and specific heat capacity, were calculated at the corresponding fluid temperature. Energy and system efficiency values were calculated using the instantaneous experimental data collected under the outdoor conditions. To smooth out the short-term fluctuations of the collected data, a 25-minute rolling average of the measured values was used in the data analysis.

Table 1: Summary of measuring instruments.

Parameter measured	Sensor type	Sensor make/model	Measurement uncertainty
Glycol supply temperature	Thermistor	METRIMA SVM TDA	±0.15% (±0.02°C)
Glycol return temperature	Thermistor	METRIMA SVM TDA	±0.15% (±0.02°C)
Tank water inlet temperature	Thermistor	ONSET S-TMB-M002	±0.2°C for 0 to 50°C
Hot water exit temperature	Thermistor	ONSET S-TMB-M002	±0.2°C for 0 to 50°C
Solar radiation	Pyranometer	S-LIB-M003	±5% (±10 W m^{-2})
Volumetric flow rate of glycol	-	METRIMA SVM F2	±0.35%
Natural gas flow rate	Diaphragm meter	AC-250	-

3   PERFORMANCE METRICS

System performance data were collected for three different modes of operation: solar energy mode, natural gas energy mode, and hybrid (solar and natural gas) mode. The following performance metrics were calculated: energy delivered to the water tank, solar fraction, collector system efficiency, gas burner efficiency, and hybrid system efficiency.

3.1 Solar Mode of Operation

In this mode of operation, water inside the storage tank is heated using solar energy only. The rate of useful energy delivered by the solar fluid to the storage tank is calculated as (Duffie & Beckman, 2013):

$$\dot{Q}_d = \dot{m}C_{p,g}(T_{fi} - T_{fo}) \tag{1}$$

The collector system efficiency is calculated as shown in Equation 2 (Duffie & Beckman, 2013). This efficiency includes not only the efficiency of the collector itself, but also heat losses between the collector and storage tank, and the effectiveness of the solar heat exchanger located inside the storage tank.

$$\eta_s = \frac{\dot{m}C_{p,g}(T_{fo} - T_{fi})}{A_c G_t} \tag{2}$$

3.2 Natural Gas Mode of Operation

In this mode of operation, water inside the tank is heated using natural gas energy. As reported by (Aldrich, 2016), the efficiency of a gas burner is calculated as:

$$\eta_{burner} = \frac{mC_{p,w}(T_{ini} - T_{fin})}{V_{gas} * HV} \tag{3}$$

In this study, efficiency values are presented for both the higher and lower heating value of natural gas.

3.3 Hybrid Mode of Operation

In this mode of operation, water inside the storage tank is heated using both solar and natural gas energy. Solar fraction in a hybrid mode is calculated as (Kalogirou, 2013):

$$f = \frac{Q_{solar}}{Q_{solar} + Q_{auxiliary}} \tag{4}$$

3.4 Uncertainty Analysis

In many cases, the desired result of a physical experiment is not directly measured but is derived using one or more directly measured variables. If a physical quantity Y is a function of n variables, X_1, X_2…, X_n, that are measured separately, assuming the measured variables as uncorrelated and random, the combined uncertainty of the derived quantity Y can be calculated as (Taylor & Kuyatt, 1994):

$$U_Y = \sqrt{\sum_{i=0}^{n} \left(\frac{\partial y}{\partial x_i}\right)^2 U_{X_i}^2} \tag{5}$$

where $\left(\frac{\partial y}{\partial x_i}\right)$ represents the partial derivative of the function $f(X_1, X_2, … X_n)$ with respect to the variable X_i and U_{X_i} represents the standard deviation of the measured variable X_i. Using this uncertainty propagation method, the uncertainty of derived variables, efficiency of collector and gas-heater efficiency, is calculated using built in capabilities of the *Engineering Equation Solver* software and reported in the following sections.

4 RESULTS AND DISCUSSIONS

4.1 Solar only heating mode

The efficiency of the solar collector heating system was measured at three initial tank temperatures of 20, 30, and 51.5°C. The final temperature in all cases was 60°C. These three cases are intended to simulate system performance for a full tank discharge and reheat ($\Delta T = 40$°C), recovery from a larger draw ($\Delta T = 30$°C), and recovery from a small draw or standby losses ($\Delta T = 8.5$°C). A summary of the results of the solar tests is shown in Table 2. Using the uncertainty propagation discussed above, the maximum uncertainty in the calculated efficiency was ±0.09%.

Figure 2 shows the solar radiation, mass flow rate of glycol, temperature difference between the glycol inlet and outlet temperature in the in-tank solar coil, tank water temperature, and collector heating system efficiency curve for a typical summer day (8/22/2017) with the storage tank initially at 20°C. Data is presented with a 25-minute rolling average applied. In this experimental run, it took approximately 6.32 hours to heat the tank water to required temperature of 60°C.

Table 2: Summary of solar tests

Initial Tank Temperature (±0.2°C)	Range of Incident Solar Flux (±10 W m^{-2})	Number of Experiments Run	Range of Time to Heat Tank (hrs.)	Range of Overall Efficiency (%)
20	780 to 860	4	5.07 to 6.45	41.8 to 43.2
30	916 to 935	4	3.72 to 4.53	38.9 to 40.5
51.5	862 to 926	4	1.15 to 2.45	34.9 to 35.2

The measured average solar radiation for the period of the experiment was 780 W m^{-2}. Depending on the intensity of solar radiation and the temperature of the water glycol fluid, the solar fluid mass flow rate varied between 42.5 and

63.7 g s⁻¹, with an average mass flow rate of 58.7 g s⁻¹. The average temperature difference between the glycol water mixture at the inlet and outlet of the tank solar coil was measured to be 10.15°C. The average efficiency of the collector heating system (defined by Equation 2) was found to be 41.83 %. The average efficiency is defined as the sum of all instantaneous (at every 10 seconds interval) efficiencies divided by the total number of data points during the solar heating time.

During the first few minutes of the test, the pump circulated the stagnant glycol water mixture to the water storage tank that had been pre-heated in the collector loop to a high temperature. This resulted in a larger than expected solar fluid temperature difference $\left(delta\ t,\ T_{fo} - T_{fi}\right)$ in the first few minutes of the test and the unusual spike at the beginning of the efficiency curve shown in Figure 2. Once the stagnant glycol water mixture was fully circulated, the solar fluid temperature difference value became stable and representative of the instantaneous solar radiation.
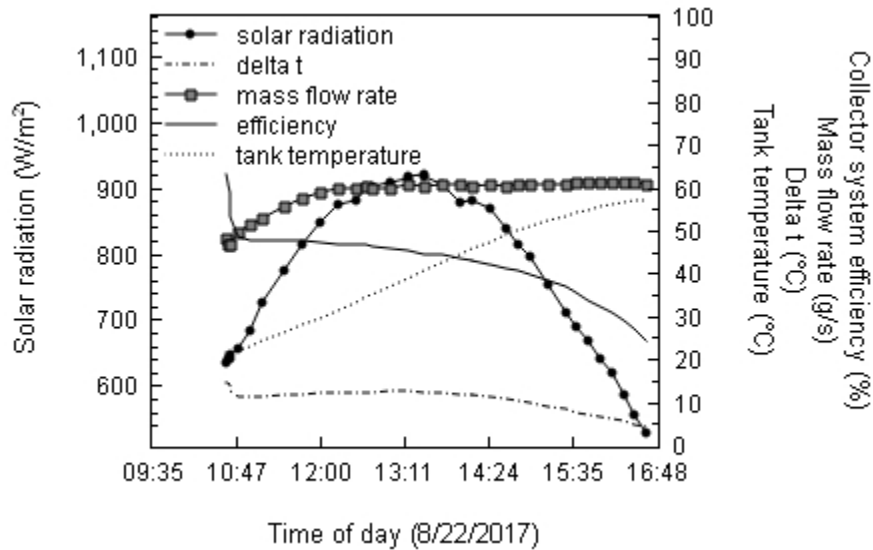

Figure 2: 25-minute rolling average of the collector system efficiency

For a steady-state operating conditions, the useful energy collected by an FPC under near normal incidence angle of solar radiation is calculated using Hottel-Whillier-Bliss equation as reported by (Duffie & Beckman, 2013):

$$Q_u = F_R A_c [G_t(\tau\alpha) - U_L(T_i - T_a)] \tag{6}$$

As per Equation 6, an FPC would collect the maximum possible energy if the temperature of fluid entering the collector (T_i) were always at a minimum possible temperature, or in other words, if the term ($T_i - T_a$) in Equation 6 was closer to zero. However, the temperature of the fluid entering the collector is not a design variable and cannot be controlled (Klein & Beckman, 1979). If we assume negligible piping heat loss and efficient heat exchange between the solar fluid and water, the collector fluid inlet temperature will be nearly equal to the storage tank temperature (Klein & Beckman, 1979). As the collector fluid inlet temperature increases, the collector heat loss value increases, and hence less energy is collected. Moreover, in real life operating conditions, we cannot assume a constant heat transfer rate between solar fluid and water. With an increase in tank water temperature and an approximately constant collector outlet temperature, the LMTD between the solar fluid and tank water decreases, reducing the efficiency of solar heat exchangers. For these two reasons, the efficiency of the collector heating decreases with an increase in tank water temperature. This efficiency reduction was experimentally observed.

Figure 3 shows the average daily efficiency of the solar collector heating system for all four tests at different initial tank water temperatures and a final tank temperature of 60°C. Taking into consideration that the average collector efficiency does not change significantly with change in solar radiation for a range of 800 to 1100 W m⁻² (Michaelides & Eleftheriou, 2011), it is seen that the efficiency of the collector heating system decreased with an increase in tank water temperature. The efficiency of the collector heating system to completely heat water to 60°C was found to be 42.01±0.09%, 39.82±0.08%, and 35.05±0.07% at initial water temperature of 20, 30, and 51.5 ±0.2°C, respectively. The reduction in efficiency with increasing inlet water temperature was expected and agrees with the trends cited in the previous literature reported by (You & Hu, 2002) and (Celuppi *et al.*, 2014).
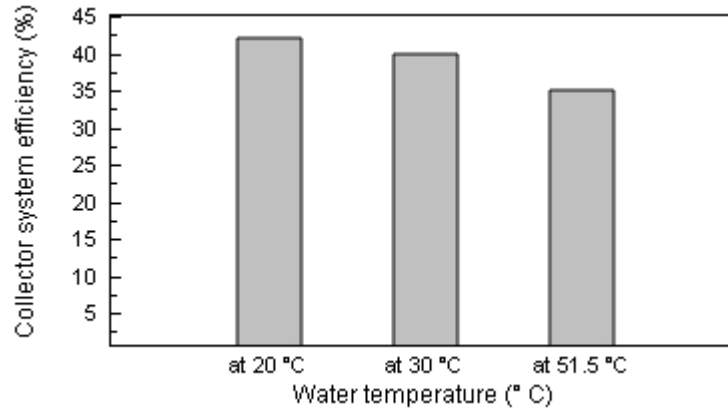
Figure 2: Collector system efficiency at different tank water temperatures

4.2 Natural gas burner efficiency at different initial water temperatures

Using natural gas only, the tank water was heated until a final temperature of 60 ± 0.2°C from three different inlet temperatures. Using Equation 3, the efficiency of the gas burner was calculated and reported in terms of higher heating value (HHV) and lower heating value (LHV) of natural gas. The higher and lower heating value of natural gas used in the calculation were 52.22 and 47.14 MJ kg^{-1}, respectively (Boundy *et al.*, 2011). The efficiency of the gas burner was found to be 69.20±0.14%, 66.41±0.13%, and 65.51±0.12% using HHV and 76.15±0.15%, 73.59±0.14%, and 72.60±0.14% using LHV for starting water temperatures of 20, 30, and 51.5±0.2°C, respectively.

Figure 3 shows the relationship between the gas burner efficiency and starting tank water temperature. It is seen that the efficiency of the gas burner is highest at an initial temperature of 20°C and, as expected, decreases with increases in initial tank water temperature. As the tank water temperature increases, the driving temperature difference (LMTD) decreases, decreasing the rate of heat transfer between combustion gases and water, and hence, reducing the gas burner efficiency. This efficiency reduction trend was expected and agrees with the trends cited in the previous literatures reported by (Maguire, 2012) and (Makaire & Ngendakumana, 2010).
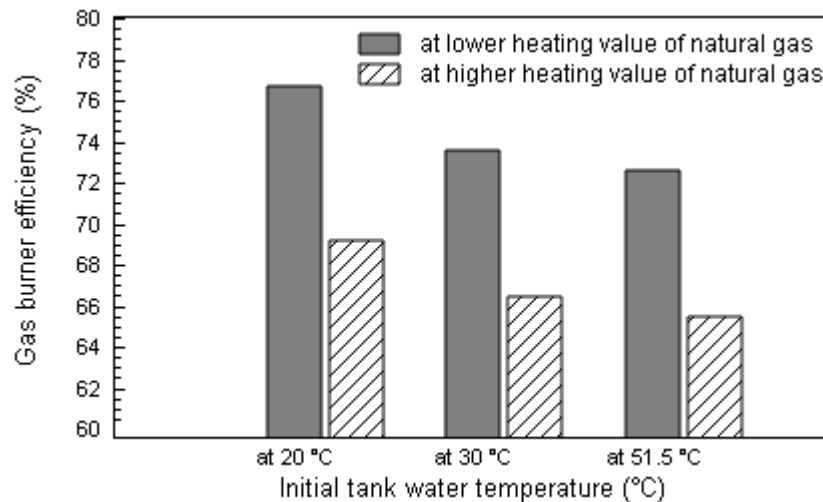

Figure 3: Natural gas burner efficiency for three different tank water temperatures

4.3 Combined Solar and natural gas

In the combined mode of heating, tank water initially at 20±0.2°C was heated to 60±0.2°C using both solar and natural gas energy, simultaneously. Four different solar radiation values representative of typical summer weather conditions in Corvallis, Oregon were used to analyze the performance of hybrid solar/gas heating system. They consisted of heavily clouded sky (8/24/2017, 11:37 am to 12:34 pm), overcast sky (8/16/2017, 3:57 pm to 4:49 pm), clear sky (8/17/2017, 12:04 pm to 12:54 pm), and intermittent cloud covered sky (8/14/2017, 1:30 pm to 2:05 pm). The average solar radiation measured during the tests were: 489±10 W/m^2 on the heavily clouded day, 616±10 W/m^2 on the

overcast day, 973±10 W/m² on the clear sky day, and 787±10 w/m² on the intermittent cloud covered day. Figure 5 shows the solar fraction and natural gas contribution at above-mentioned four solar radiation values. It is seen that with an increase in average solar radiation value, a larger solar fraction is achieved, and hence less natural gas energy is required. However, as the solar fraction increases, and the energy contributed by natural gas decreases, the efficiency of the gas burner also decreases due to the reduction in LMTD, as discussed above. Based on the higher heating value of natural gas, the gas burner efficiency was found to be 69.08, 66.80, 66.17, and 65.18% at solar fractions of 4.93, 9.40, 11.39, and 14.27%, respectively.
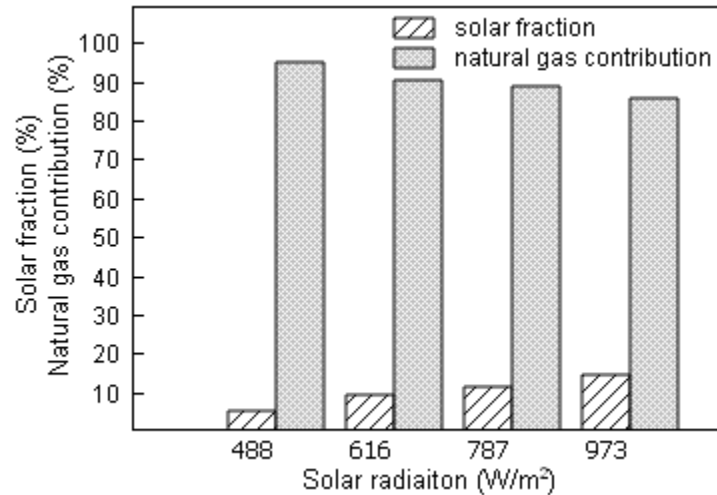
Figure 4: Solar fraction at different solar radiation values

This set of experiments was conducted using the baseline control strategy where both natural gas and solar energy were used together to minimize tank heating time. In a real application, one may institute more sophisticated controls to use solar energy to heat the tank to as high a temperature as possible, and then use gas to finish heating, thus increasing the solar fraction. However, even using this control strategy would result in lower burner efficiency due to the decreased LMTD.

5 POTENTIAL IMPROVEMENTS OF HYBRID SYSTEM

According to ASHRAE (ASHRAE, 2011), the annual domestic hot water (60°C) demand of a typical US family is 86,140 liters. Using the experimental burner efficiency values, the volume of natural gas consumed by the solar/gas hybrid system to satisfy this hot water demand for varying initial tank temperatures and solar fractions was approximated. Three inlet tank water temperature (20, 30, and 51.5°C) scenarios were considered. The final water temperature was assumed to be 60°C. For each inlet temperature, five different solar fractions (0, 25, 50, 75, and 100%) were assumed and the volume of natural gas consumed at corresponding solar fraction was calculated as:

$$V_{gas} = (1-f)\frac{mC_{p,w}(T_{ini} - T_{fin})}{\eta_{burner} * HV} \tag{7}$$

The average volume of natural gas consumed by the hybrid system per degree temperature rise is shown in Table 3 below. It is seen that for a higher initial tank water temperature, a larger amount of natural gas is required per degree temperature rise. Hence, it is clear that lower inlet water temperature is desired to maximize gas burner efficiency and overall hybrid system efficiency.

Based on the experimental study of the performance of the solar/gas hybrid system, there is clearly an opportunity to explore new system configurations that maximize solar fraction while also maximizing the efficiency of the gas auxiliary unit. Under the current operation configuration of the hybrid system, the solar fraction can be maximized by using solar energy to heat the storage tank water to the required temperature, and when the solar input is not sufficient, auxiliary gas burner turns on to top up the tank water temperature. However, as observed experimentally, the efficiency of the gas burner decreases at higher starting water temperature, resulting in higher gas consumption. So, to avoid this inefficiency, it is suggested that instead of heating pre-heated tank water, the incoming cold water should be heated separately by the gas burner and mixed with the hot water exiting the solar storage tank. This can be achieved by using a tankless gas-fired water heater and a thermostatic mixing valve as shown in Figure 6. A storage gas heater can be

Table 3: Natural gas consumption in cubic meters per degree Celsius temperature rise

Solar fraction (%)	At 20 °C Burner efficiency = 69.23%	At 30 °C Burner efficiency = 66.43%	At 51.5 °C Burner efficiency = 65.50%
0	12.82	13.36	13.55
0.25	9.61	10.02	10.16
0.5	6.41	6.68	6.77
0.75	3.20	3.34	3.39
1	0.00	0.00	0.00

used as an alternative to instantaneous burner. However, tankless water heaters have higher combustion efficiencies and eliminate standby losses that are common to storage type water heaters (Hoeschele & Springer, 2008).

The operation of the thermostatic mixing valve can be controlled by using temperature sensors. A thermal-sensitive mechanism within the valve's body automatically proportions the amount of hot water coming out of the solar heater and gas burner. The valve can be programmed in a way that when the temperature of water exiting the solar tank falls below a minimum required temperature, the gas burner turns on to produce the required temperature blend. As observed experimentally, solar energy is usually enough to completely heat the tank to the required temperature during summer months. In summer, a hot water draw usually can be made from solar storage tank alone. In contrast to this, solar fraction is typically low during winter months. So, a major proportion of hot water demand would be provided by gas heater during winter.
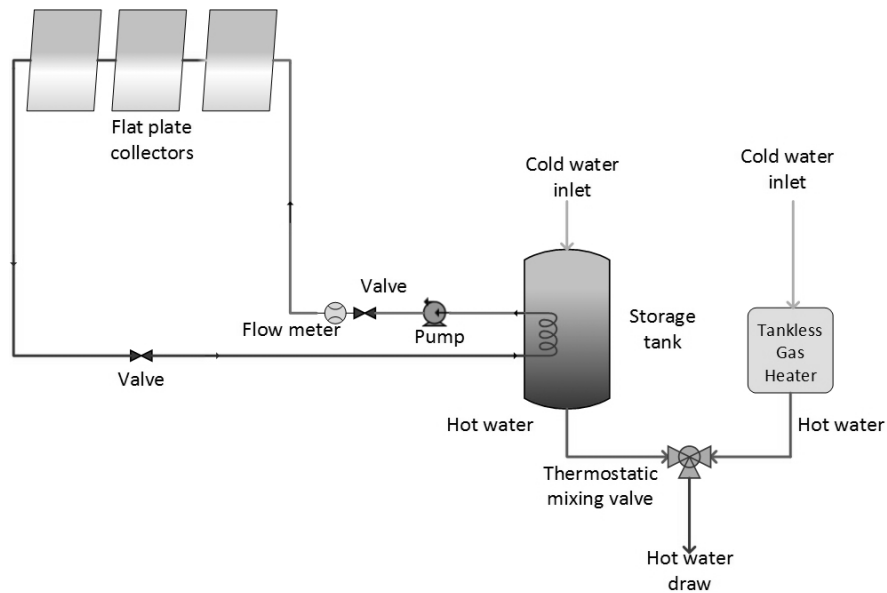
Figure 6: Proposed operation configuration

The volumes of natural gas consumed by the solar/gas hybrid system under the current and proposed configurations to satisfy annual hot water demand for a typical US family were calculated using Equation 7 and shown in Figure 7. Two gas burner types, a tankless instantaneous gas burner and the existing storage type gas burner, were considered under the proposed configuration. The tank inlet water temperature and final water temperature were assumed to be 20 and 60°C, respectively. Five different solar fractions (0, 25, 50, 75, and 100%) were assumed. It is seen that less natural gas is consumed under the proposed configuration for both instantaneous and existing burner compared to current configuration, particularly in low and midrange (0 to 25%) of solar fraction, which is typical of winter or spring season operation. Under the proposed configuration, the gas burner is always heating incoming cold water, thus operating at maximum possible efficiency. Savings offered by the proposed configuration with an instantaneous gas burner are higher than with the existing gas burner because of the higher thermal efficiency (Healy, 2015). The initial installation cost of the instantaneous gas-fired water heater is usually higher than traditional storage water heater. But, instantaneous water heaters typically last longer and have lower energy costs, which could justify its higher installation cost.
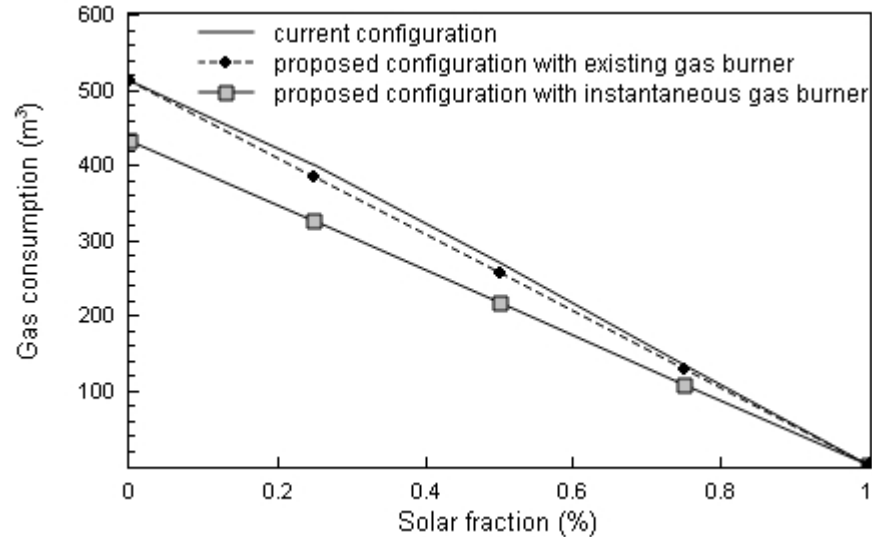
Figure 7: Approximate annual volume of natural gas consumed by the hybrid system under current and proposed configuration

6 CONCLUSION

Performance of a solar/gas hybrid water heating system installed in Corvallis, Oregon was monitored for typical summer weather conditions. The hybrid system was operated using three different modes of heating: solar, gas, and combined solar/gas mode, using different temperature lifts and solar insolation values. In the solar heating mode, the efficiency of the collector heating system was found to be 41.97%, 39.82%, and 35.05% at starting water temperatures of 20, 30, and 51.5°C, respectively. For the natural gas heating mode, the starting tank water temperature was found to have a significant impact on the efficiency of the gas burner. For starting tank water temperatures of 20, 30, and 51.5°C, the efficiency of the gas burner was found to be 69.2%, 66.4%, and 65.5% at the HHV and 76.7%, 73.6%, and 72.6%, respectively, at the LHV of natural gas. In the combined solar/gas heating mode, the gas burner efficiency decreased with increases in solar fraction. For solar fractions of 4.93, 9.40, 11.39, and 14.27%, the gas burner efficiency was found to be 69.08, 66.8, 66.17, and 65.18 %, respectively, in terms of the HHV of natural gas. Based on experimental observations of the hybrid system, a configuration with better thermal performance is suggested where incoming cold water is heated separately and mixed with the solar tank water using a thermostatic mixer.

NOMENCLATURE

A_C	Collector aperture area	(m²)
C_P	Specific heat	(J kg⁻¹ K⁻¹)
F_R	Collector heat removal factor	-
G_t	Solar irradiance	(W m⁻²)
U_L	Collector overall heat transfer coefficient	(W m⁻² C⁻¹)
T	Temperature	(°C)
$\dot{m}$	Mass flow rate	(kg s⁻¹)
$\dot{Q}$	Rate of energy	(J s⁻¹)
V	Volume	(m³)
HV	Heating value	(kJ m⁻³)
Q	Energy	(J)
F	Solar fraction	(%)
A	Area of heat exchanger	(m²)
U	Heat exchanger overall heat transfer coefficient	(W m⁻² C⁻¹)
$LMTD$	Logarithmic mean temperature difference	(°C)

Greek

η	Efficiency
τ	Transmittance
α	Absorptance

Subscripts

U	Useful		*D*	Delivered
I	Inlet		*S*	System
A	Ambient		*Burner*	Natural gas burner
G	Glycol		*W*	Water
Co	Collector outlet		*Ini*	Initial
Ci	Collector inlet		*Fin*	Final
Fi	Fluid inlet		*Gas*	Natural gas
Fo	Fluid outlet		*Solar*	Solar heating system
C	Collected		*auxiliary*	Auxiliary heating system

REFERENCES

Aldrich, R. (2016). *Indirect Solar Water Heating in Single-Family, Zero Energy Ready Homes*. NREL (National Renewable Energy Laboratory (NREL), Golden, CO (United States)).

Ayompe, L. M., & Duffy, A. (2013). Analysis of the thermal performance of a solar water heating system with flat plate collectors in a temperate climate. *Applied Thermal Engineering*, *58*(1), 447–454.

Bill Healy. (2015). Water Heating Technologies and Ratings. National Institute of Standards and Technology. Retrieved from https://www.nist.gov/sites/default/files/documents/iaao/Healy.pdf

Boundy, R. G., Diegel, S. W., Wright, L. L., & Davis, S. C. (2011). *Biomass Energy Data Book: Edition 4*. Oak Ridge National Laboratory (ORNL).

Celuppi, R., Scapinello, J., Andrade, F. G., Revello, J. H., & Magro, J. D. (2014). Solar energy use for water pre-heating in boilers of agro-industries. *Engenharia Agrícola*, *34*(3), 451–460.

Duffie, J. A., & Beckman, W. A. (2013). *Solar engineering of thermal processes*. John Wiley & Sons.

Fronk, B. M., & Keinath, C. M. (2017). Comparison of Primary Energy Consumption of Vapor and Non-Vapor Compression Natural Refrigerant Heat Pumps for Domestic Hot Water Applications. In *12th IEA Heat Pump Conference 2017*.

AHSRAE. (2011). Heating, Ventilating, and Air-Conditioning Applications. *American Society of Heating, Refrigerating and Air-Conditioning Engineers, Inc*.

ASHRAE. (2008). Ventilating, and Air-Conditioning Systems and Equipment (IP Edition). *American Society of Heating, Refrigerating and Air-Conditioning Engineers, Inc*.

Hoeschele, M. A., & Springer, D. A. (2008). Field and Laboratory Testing of Gas Tankless Water Heater Performance. *ASHRAE Transactions*, *114*(2), 453–461.

Kalogirou, S. A. (2013). *Solar energy engineering: processes and systems*. Academic Press.

Klein, S. A., & Beckman, W. A. (1979). A general design method for closed-loop solar energy systems. *Solar Energy*, *22*(3), 269–282.

Maguire, J. B. (2012). *A parametric analysis of residential water heaters*. University of Colorado at Boulder.

Makaire, D., & Ngendakumana, P. (2010). Thermal performance of condensing boilers.

Michaelides, I. M., & Eleftheriou, P. C. (2011). An experimental investigation of the performance boundaries of a solar water heating system. *Experimental Thermal and Fluid Science*, *35*(6), 1002–1009.

Monthly Energy Review - Energy Information Administration. (2018). Retrieved from https://www.eia.gov/totalenergy/data/monthly/#prices

Rodriguez-Hidalgo, M. C., Rodríguez-Aumente, P. A., Lecuona, A., & Nogueira, J. (2012). Instantaneous performance of solar collectors for domestic hot water, heating and cooling applications. *Energy and Buildings*, *45*, 152–160.

Taylor, B. N., & Kuyatt, C. E. (1994). *Guidelines for evaluating and expressing the uncertainty of NIST measurement results*. US Department of Commerce, Technology Administration, National Institute of Standards and Technology Gaithersburg, MD.

You, Y., & Hu, E. J. (2002). A medium-temperature solar thermal power system and its efficiency optimization. *Applied Thermal Engineering*, *22*(4), 357–364.